Available online at www.sciencedirect.com
ScienceDirect
Journal of the European Ceramic Society 31 (2011) 3153–3158
www.elsevier.com/locate/jeurceramsoc

Synthesis and study on phase diagram of 1–10 mol% SnO_2–doped Bi_2O_3

Tzu-Chi Kuo, Yu-Lin Kuo [a], Wen-Cheng J. Wei *

Department of Materials Science and Engineering, National Taiwan University, 1 Roosevelt Rd., Section 4, Taipei 106, Taiwan, ROC

Available online 23 June 2011

Abstract

Bi_2O_3 materials doped with various SnO_2 concentrations were prepared by colloidal process and solid state reactions to achieve high density and uniform microstructure. Thermal behavior, and crystalline phases of the SnO_2–doped Bi_2O_3 (BSO) samples were investigated by differential thermal analyses, X-ray diffraction, and scanning electron microscopy. A new phase diagram of Bi_2O_3–(1–10 mol%) SnO_2 system is proposed in this study. The results show that 1 mol% SnO_2 doped concentration is totally dissolved in Bi_2O_3 without the existence of any impurity phases as compared to higher doping SnO_2 concentration.

Keywords: Bi_2O_3; SnO_2; Electrolyte; Fuel cell; Phase diagram

1. Introduction

Intermediate-temperature solid oxide fuel cell (IT-SOFC) has been developed to solve the problems associating with the operation of the ZrO_2-based fuel cells at high temperatures (>800 °C). Degradation of metallic and glassy materials, introduction of thermal stresses, and inter-diffusion between cell parts are always associated with the high operation temperature and have been greatly concerned in the past decade. Yttria-doped zirconia (YSZ) had been the most common electrolyte material for SOFC, and became a challenge if used at the temperatures <650 °C due to its poor conductivity. Researches in the last decade have been conducted to develop new kinds of the electrolyte to replace YSZ. One of the candidates is stabilized Bi_2O_3 and its derivatives.

The main interest in the stabilized Bi_2O_3 materials arises from a high ionic conductivity of δ-phase Bi_2O_3, which originates from[1–4]:

(1) high polarizability of Bi cation network and highly disordered anion network lead to high O^{2-} mobility;
(2) high concentration of intrinsic oxygen vacancy in the fluorite structure, up to 25% of the oxygen sites;
(3) good accommodating capability of alio-valent cations into the matrix with highly disordered surroundings.

Many Bi_2O_3–MO binary systems have been reported in literature, in which the used MO_x dopant is either alkaline earth oxide, rare-earth oxide, pentavalent oxide (M=V, Nb, Ta), or heavy element oxide (for example, M=W or Mo). Those systems showing stabilized fluorite structure (δ-structure) or rhombohedral structure (γ-structure) have a good electric conductivity property.[1–3] Among these, the highest conductivity of 20 mol% Er_2O_3–doped Bi_2O_3 (ESB) reported by Wachsman's group[5] reaches 0.23 S/cm at 600 °C. Another example is 5 mol% ZrO_2 doped in Bi_2O_3 system. The existence of ZrO_2 is proven to kinetically stabilize δ-structure which cannot sustain long-term thermal treatment originally.[6]

Two possible defect reactions of ZrO_2 in $Bi_2O_3$are:

$$\frac{3}{2}ZrO_2 \rightarrow \frac{3}{2}Zr^{\bullet}_{Bi} + 3O^{x}_{O} + \frac{1}{2}V'''_{Bi} \quad (1)$$

$$2ZrO_2 + V^{\bullet\bullet}_{O} \rightarrow 2Zr^{\bullet}_{Bi} + 4O^{x}_{O} \quad (2)$$

Fung et al.[6] reported the later one was likely to occur since a high oxygen vacancy concentration existing in Bi_2O_3.

However, these doped-Bi_2O_3 electrolyte materials are possibly unstable in the reducing atmosphere. For example, Wachsman et al.[7] reported that Bi metal would form as Er-stabilized Bi_2O_3 material tested in H_2/H_2O atmosphere although it can stable at an oxygen partial pressure as low as 10^{-20} atm in the Ar/O_2 atmosphere. They also claimed that the existence of

* Corresponding author. Tel.: +886 2 33661317; fax: +886 2 23634562.
E-mail address: wjwei@ntu.edu.tw (W.-C.J. Wei).
[a] Now joint Department of Mechanical Engineering, National Taiwan University of Science and Technology.

0955-2219/$ – see front matter © 2011 Elsevier Ltd. All rights reserved.
doi:10.1016/j.jeurceramsoc.2011.05.012

Table 1
Bi_2O_3 phase transition temperature reported in literature.

Phase transition temperature (°C)		Reference
α–δ	δ–L	
729	824	Shuk et al.[3]
730	Over 825	Kargin et al.[11]
730	825	Galakhov[12]
740	825	Asryan et al.[13]
730	800	Levin et al.[14]
727	N/A	Rao et al.[15]
729	824	Harwig and Gerards[16]

H_2 would kinetically reduce Bi_2O_3. One of proposed methods to solve the problem was using a thin YSZ layer to protect the doped-Bi_2O_3 electrolyte.[2,6]

Fung et al.[6] proposed that other tetravalent dopants have similar kinetically stabilized effect as ZrO_2 in Bi_2O_3 matrix. Since they reported that the stabilization effect was due to the formation of cation interstitial. And the ionic radius of Sn^{4+} (0.069 nm) is similar to the radius of Zr^{4+} (0.072 nm), and might have same conductive mechansim.[8,9] The doping of SnO_2 into Bi_2O_3-based system has a similar effect on Bi_2O_3 as the case being doped by ZrO_2. According to the possible defect reaction:

$$2SnO_2 + V_O^{\bullet\bullet} \rightarrow 2Sn_{Bi}^{\bullet} + 4O_O^x \quad (3)$$

the concentration of the oxygen vacancy is reduced when the tetravalent cation is doped into Bi_2O_3. Thus, the interaction between oxygen vacancies is less likely and possibility of the formation of defect cluster is decreased.

Another advantage of SnO_2 is the stability of the oxide in hydrogen-assisted reducing atmosphere. Hoflund[10] reported that SnO_2-based materials are fairly inert to a strongly reductive treatment by 40 Torr of H_2 at 200 °C as holding for 1 h. The stability in reducing atmosphere was due to the existence of valence transition of the composition between SnO and SnO_2.

According to the Bi_2O_3–SnO_2 phase diagrams reported in literature, one intermediate phase $Bi_2Sn_2O_7$ and a eutectic point at Bi_2O_3-rich side are noted. No obvious SnO_2 solid solutions near the Bi_2O_3-rich side are reported.[11–14] However, several discrepancies are found existing between those phase diagrams. They are:

(1) The phase diagram published by Kargin et al.[11] shows a solidus line located at the temperature range of 790–825 °C as the SnO_2 concentration is lower than 66.7 mol%. However, the curve does not exist in the other phase diagrams.[12–14]
(2) The transition temperature of α–δ phase and melting temperature of pure Bi_2O_3 reported in literature are different, as summarized in Table 1. The possible α–δ phase transition temperature is 730 °C, and melting temperature is 825 °C.
(3) Different positions of liquidus line near the Bi_2O_3-rich side. For example, 10 mol% SnO_2–doped Bi_2O_3 can melt completely at 900 °C according to the phase diagrams reported by Galakhov[12] and Asryan et al.[13], while the material still stay as solid phase according to the diagrams reported by Kargin et al.[11] and Levin et al.[14]

A careful study in the region containing 0–10 mol% SnO_2 between 500 and 1000 °C is need. This study is planned to understand the phase transition behavior of 1–10 mol% SnO_2–doped Bi_2O_3, so to find an appropriate composition which can stabilize δ-phase, and to find a composition performing a good electrical conductivity at 500–650 °C.

2. Experimental procedures

Bi_2O_3 powder (99.99%, Alfa Aesar, USA) and SnO_2 powder (99.9%, Alfa Aesar, USA) were used to prepare $Bi_2Sn_2O_7$ phase and variousSnO_2–doped Bi_2O_3samples. The dopant molar ratio and the name of the sample are abbreviated as 0.5BSO, 1BSO, 2BSO, 4BSO, 6BSO, and 10BSO. D-134 (ammonium salt of homo-polymer of 2-propenoic acid, Dai-ichi, Japan) was chosen as the dispersant for both oxide powders.[17] The flowchart of the experimental steps is shown in Fig. 1. Bi_2O_3 slurries at 28 vol.% solid loading and SnO_2 slurries at 25 vol.% solid loading were individually prepared by mixing with de-ionized water and 2 wt.% D-134 (based on powder), and then ball-milling for 24 h. Two dispersed slurries were consequently mixed according to specified molar ratio. The mixed slurries were placed in a turbo mixer for 2 h to reach homogeneity, then dried by a rotary vacuum evaporator. Dried mixtures were calcined at 700 °C for 1 h and ground to passed 220 mesh screen. Die-pressing was used to make green pellets for the following experiments. 2 g powder as a batch was preloaded in WC die and die-pressing by the steps using a pressure of 12 MPa holding for 1 min, then 27 MPa for 2 min. The green pellets were sintered at 800 °C for 2 h in air.

To investigate the phase transition and crystalline behavior of the samples, differential thermal analyzer (DTA, SDTQ600, TA Waters LLC, USA) was used to investigate the phase transition behaviors of the samples. Powder samples were placed in Pt crucible in air, and heated to 850 °C at a ramping rate of 10 °C/min or 2 °C/min. While an X-ray diffractometer (XRD, Rigaku TTRAX 3) was used to study the formation of crystalline phases and to quantify the phases of the samples. The scanning was carried on from 20° to 60° with a step of 0.02° and a scan speed of 4°/min or 1°/min. Owing to the coexistence of α-Bi_2O_3 and $Bi_2Sn_2O_7$ phases in the Bi_2O_3–SnO_2 phase diagram[11–14], the quantification of SnO_2 content in BSO samples by the X-ray intensity–concentration calibration line for Bi_2O_3 and $Bi_2Sn_2O_7$ was firstly made. The standard samples of pure Bi_2O_3 and $Bi_2Sn_2O_7$ mixture with various molar ratios were prepared by simply grinding/mixing in ethanol solution. The integral intensities of strongest peaks of the two phases were used to calculate the relative concentrations.

Archimedes' method was employed to get the density of sintered samples. The theoretical densities were calculated based on the mixing rule of two pure oxides according to the specified molar ratio of Bi_2O_3 and SnO_2.

Scanning electron microscope (SEM, JSM 6510, JEOL, Japan) was used to observe detail microstructure. The sintered

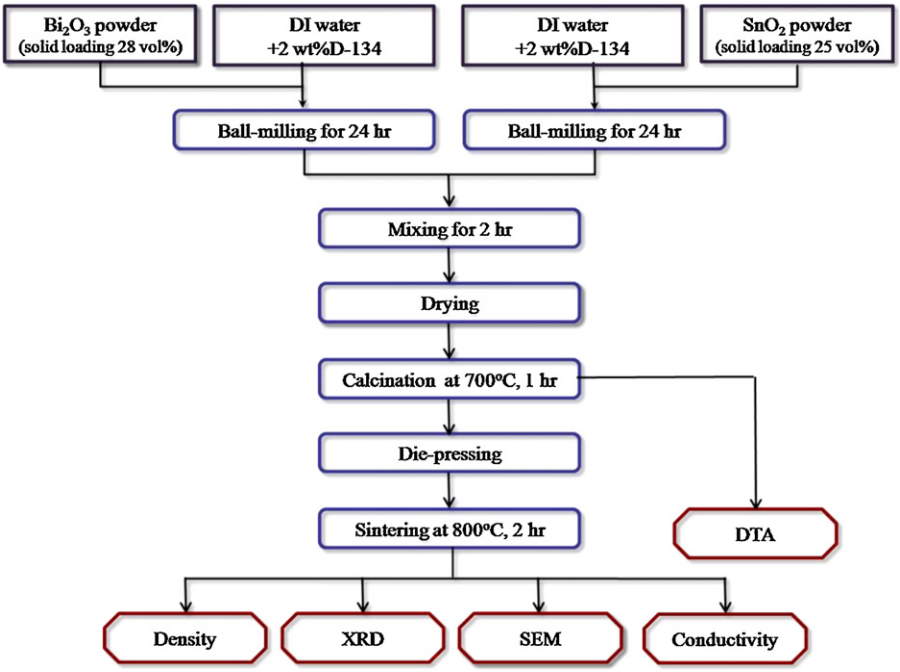

Fig. 1. Experimental flowchart of the SnO_2–doped Bi_2O_3 samples prepared in this study.

specimens were polished using SiC abrasive papers, and then cleaned in alcohol by ultrasonic cleaner. After drying, the surfaces of the samples were coated with thin Pt film so makes the sample electric conductive for SEM observation.

3. Results and discussion

3.1. Phase transition of SnO_2–doped Bi_2O_3

Thermal behavior of BSO samples was investigated by selecting a melting temperature 825.0 °C of pure Bi_2O_3 as the standard temperature for all DTA tests. Two phase transition temperatures, T_{t1} and T_{t2}, were observed in all samples. Compared to the Bi_2O_3–SnO_2 phase diagram[11–14], the T_{t1} temperature corresponds to the phase transition of α- to δ-Bi_2O_3 phase. T_{t2} was recognized as the melting point of a binary composition. The solidus line referred in the report of Kargin et al.[11] was not observed in this study. The average phase transition temperature of α- to δ-phase (T_{t1}) is 725.6 ± 1.4 °C, and melting point (T_{t2}) is 827.3 ± 1.5 °C, as shown in Table 2. The deviations possibly came from the instrumental error and compositional inhomogeneity of the testing samples. Statistical method[18], i.e., t-distribution, was used to analyze the phase transition temperatures at a heating rate of 10°/min. The mean value, standard deviation (StDev), and 90% confidence interval (90% CI) of T_{t1} and T_{t2} values are summarized in Table 2.

The effect of heating rate on the thermal behaviors of BSO samples was also investigated by DTA. As seen in Fig. 2, T_{t1} = 725.9 °C and T_{t2} = 827.7 °C at a heating rate of 2°/min were also obtained for 2BSO sample. Compared to the results of 2BSO samples by a heating rate of 10°/min, the effect of different heating rates on the α- to δ-phase transition and melting temperature is not apparent. This result implies that the data measured at the 10 °C/min or 2 °C/min are reliable.

An endothermic peak as the arrow indicated in Fig. 2 was found in all DTA curves of BSO samples other than the peak representing the α- to δ-phase transition, but the peak was not observed in the results of pure Bi_2O_3. Since the γ-phase $Bi_2Sn_2O_7$ is stable from 690 °C to above 1000 °C[13,19], the existence of the peak should be the dissolution of SnO_2 into the Bi_2O_3 matrix.

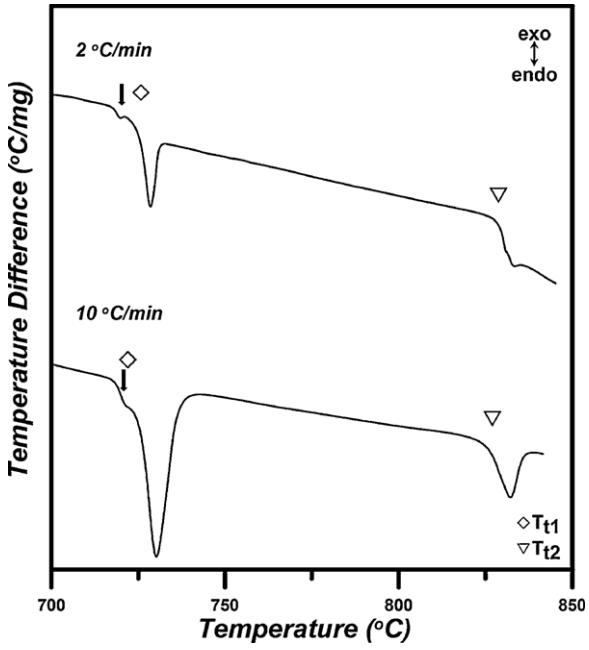

Fig. 2. DTA results of 2BSO samples at different heating rates.

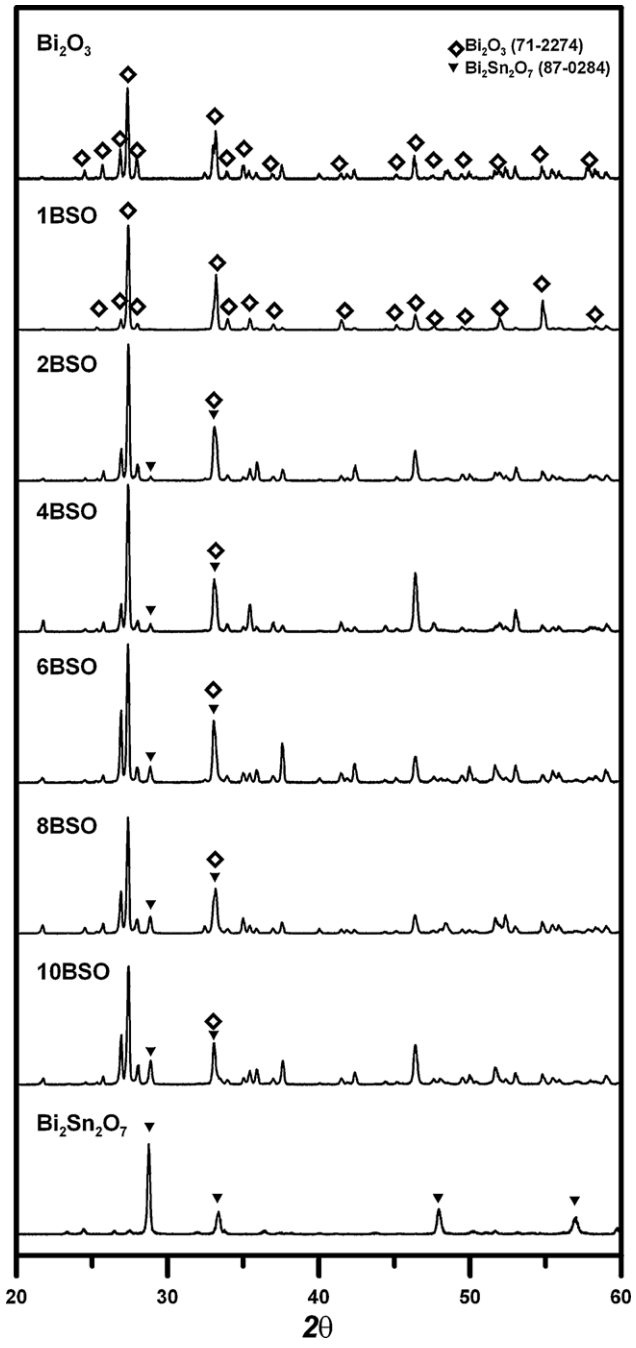

Fig. 3. X-ray diffraction patterns of BSO samples sintered at 800 °C for 2 h.

Two crystal phases of sintered BSO samples determined from the XRD spectra have been identified, either monoclinic Bi_2O_3 (α-Bi_2O_3) or cubic $Bi_2Sn_2O_7$ (γ-$Bi_2Sn_2O_7$), as shown in Fig. 3. The major peaks of all BSO samples are α-phase Bi_2O_3, while the intensity of $Bi_2Sn_2O_7$ phase increases with increasing SnO_2 content. As 1 mol% SnO_2 is doped in Bi_2O_3 matrix, only α-Bi_2O_3 peaks are observed. In order to do an accurate identification of 1BSO sample, slower scanning rate of 1°/min was performed (the data not shown herein). $Bi_2Sn_2O_7$ phase is not observed in 1BSO sample even scan with the low speed, indicating that 1 mol% SnO_2 completely dissolve in Bi_2O_3 matrix.

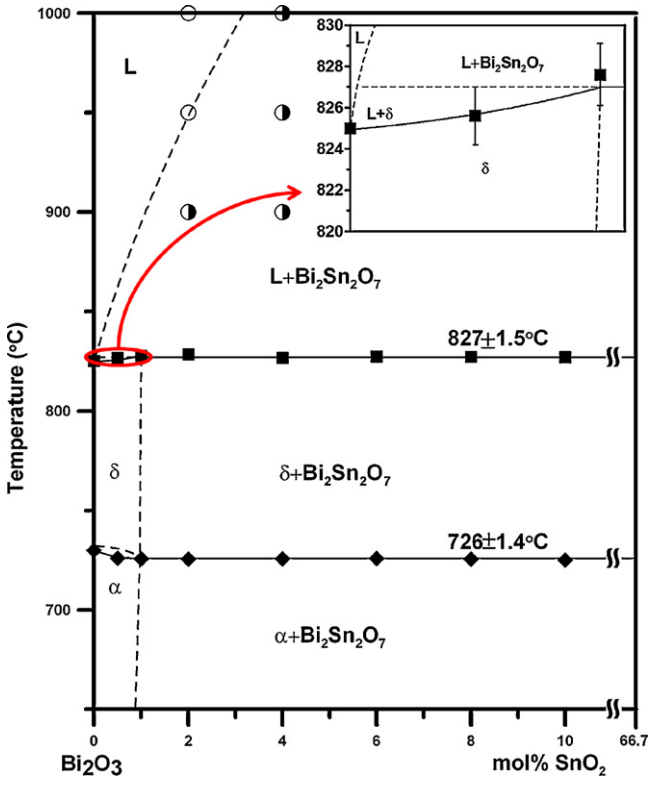

Fig. 4. Bi_2O_3–SnO_2 phase diagram illustrating the region with 0–10 mol% SnO_2. The insert shows the melting point of pure Bi_2O_3 and the peritectic point of δ-phase to L + $Bi_2Sn_2O_7$ transition.

Fig. 4 shows a proposed Bi_2O_3–SnO_2 phase diagram in the region of 1–10 mol% SnO_2. The difference of phase transition temperature of pure Bi_2O_3 and BSO samples is conjectured to be the effect of SnO_2–dissolution in Bi_2O_3. From the DTA analysis results listed in Table 2,the melting point raises to a higher value (827.3 ± 1.5 °C) as slightly SnO_2 was doped, which is not seen in those Bi_2O_3–SnO_2 phase diagrams.[11–14] The phase transition behavior of the samples with 0–1 mol% SnO_2 region was speculated similar to that shown in Bi_2O_3–ZrO_2 phase diagram.[14] The location of liquidus line was decided according to the crystalline conditions of quenched samples from 900 to 1000 °C, which were examined by XRD.

3.2. Properties of sintered BSO samples

The XRD intensity of various concentrations of $Bi_2Sn_2O_7$ in the mixture of Bi_2O_3 and $Bi_2Sn_2O_7$ was used to quantify the SnO_2-content in sintered BSO samples. The integral intensities of maximum peaks of two phases, corresponded to {1 2 0} of Bi_2O_3 ($2\theta = 27.4°$) and {2 2 2} of $Bi_2Sn_2O_7$ ($2\theta = 28.8°$), were calculated. The calibration curve of Bi_2O_3–$Bi_2Sn_2O_7$ was obtained from the standard samples (not shown herein). The intensity ratios, $I_{Bi_2Sn_2O_7}/I_{Bi_2O_3} + I_{Bi_2Sn_2O_7}$, of sintered BSO samples are obtained from the XRD results in Fig. 3. According to the Bi_2O_3–MO_x phase diagrams, the amounts of oxides which can dissolve in Bi_2O_3 matrix are less than 1 mol% in most cases. The solubility of the M_2O_5 (M=V, Nb, etc.) in Bi_2O_3 matrix is

Table 2
Quantitative results of BSO sample analyzed by DTA.

Sample name	T_{t1} (°C)			T_{t2} (°C)		
	Mean (°C)	StDev (°C)	90% CI[a] (°C)	Mean (°C)	StDev (°C)	90% CI[a] (°C)
Bi_2O_3	730.0	–	–	825.0	–	–
0.5BSO	726.0	0.6	725.3–726.8	826.6	1.4	824.9–828.2
1BSO	725.7	1.5	724.0–727.5	827.6	1.6	825.8–829.4
2BSO	725.6	1.4	724.0–727.3	828.2	1.5	826.5–830.0
4BSO	725.7	1.5	724.0–727.4	826.6	1.5	824.9–828.3
6BSO	725.8	1.4	724.2–727.4	827.2	1.3	825.6–828.8
8BSO	725.6	1.3	724.0–727.1	827.1	1.6	825.1–829.0
10BSO	725.1	1.3	723.6–726.6	826.9	1.6	825.0–828.7
1∼10BSO	725.6	1.4	–	827.3	1.5	–

[a] 90% confidence internal (CI): there are 90% of the measured results, which are measured by same steps, fall in the interval.

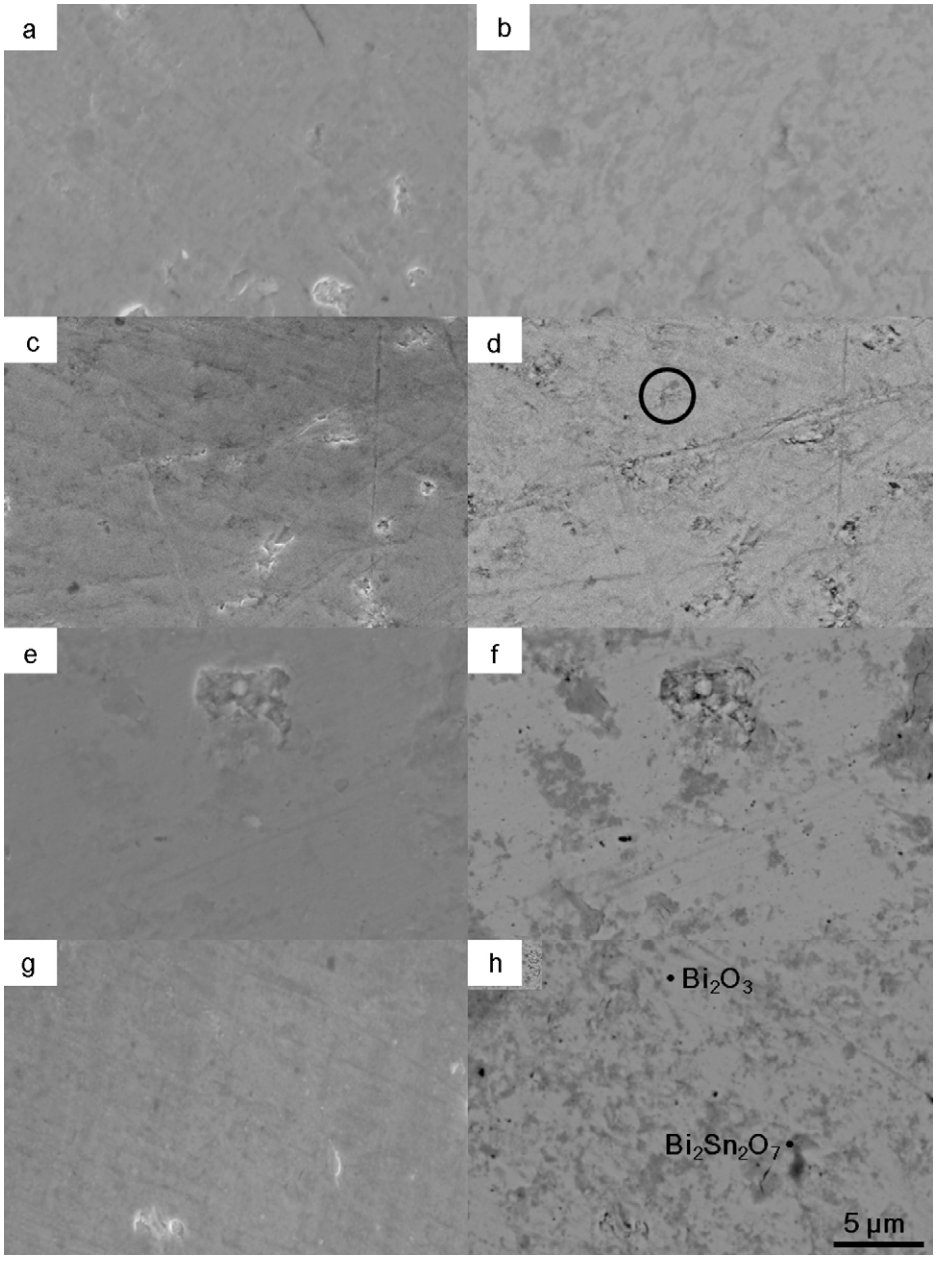

Fig. 5. SEM microstructures of polished BSO samples sintered at 800 °C for 2 h. (a) 1BSO by secondary electron (SE) mode, (b) 1BSO by back-scattered electron (BSE) mode, (c) 2BSO by SE mode, (d) 2BSO by BSE mode, (e) 6BSO by SE mode, (f) 6BSO by BSE mode, (g) 10BSO by SE mode, and (h) 10BSO by BSE mode.

about 2.5 mol%, which is higher than other oxides.[14] But none of solubility range of Bi_2O_3 in $Bi_2Sn_2O_7$ are reported in literature.

For electrolyte application in SOFC, density is one of important properties for the electrolytes, of which the porosity should be less than 10%. The apparent bulk densities of sintered BSO samples are ~95%, which are high enough to prevent the crossover of fuel gases and the oxidant.

Fig. 5 shows the microscopic pictures of the polished surfaces of sintered BSO samples. Phase separation of $Bi_2Sn_2O_7$ in Bi_2O_3 matrix can be examined by back-scattered electron (BSE) mode, and proven by energy-dispersive spectroscopy (EDS) in the 2BSO–10BSO samples. For 1BSO sample, homogeneous solid solution could be assured by BSE mode. Apart from 1BSO sample, the existence of two-phase microstructure can be observed in the SEM micrographs. The tendency that the amount of $Bi_2Sn_2O_7$ phase increase as SnO_2-doped molar ratio is also shown. The SEM images are consistent with the XRD results of Fig. 3.

XRD and SEM results indicated that about 1 mol% SnO_2 was totally dissolved in Bi_2O_3 matrix, in accordance to the proposed new Bi_2O_3–(10 mol%) SnO_2 phase diagram. The phase diagram consists of two-phase (L + δ-phase) region, a solid-soluted δ-phase region, and a peritectic temperature at 827 °C, as shown in the insert of Fig. 4.

4. Conclusions

The phase transition behavior of 1–10 mol% SnO_2–doped Bi_2O_3 samples has been investigated. The DTA results showed that α–δ phase transition temperature is 726 ± 1.5 °C, and peritectic point of δ-phase to L + $Bi_2Sn_2O_7$ transition is 827 ± 1.6 °C. While XRD and SEM results showed that the 2nd phase ($Bi_2Sn_2O_7$) existed in all BSO samples except of 1BSO. The modified binary phase diagram is proposed, as shown in Fig. 4.

The sintered single-phase 1BSO sample is dense (>95.0% T.D.). Uniform microstructure of BSO samples consisted of α-Bi_2O_3 and $Bi_2Sn_2O_7$ grains. Doping of Sn^{4+} cation into Bi_2O_3 could not stabilize the δ-phase, but transform to α-phase below 726 °C.

Acknowledgement

The authors like to thank the funding offered by National Science Council in Taiwan by the contract number NSC-98-2811-E-002-062.

References

1. Sammes NM, Tompsett GA, Näfe H, Aldinger F. Bismuth based oxide electrolytes-structure and ionic conductivity. *J Eur Ceram Soc* 1999;**19**(10):1801–26.
2. Azad AM, Larose S, Akbar SA. Bismuth oxide-based solid electrolytes for fuel cells. *J Mater Sci* 1994;**29**:4135–51.
3. Shuk P, Wiemhdferb HD, Guth U, Gijpeld W, Greenblatt MM. Oxide ion conducting solid electrolytes based on Bi_2O_3. *Solid State Ionics* 1996;**89**(3–4):179–96.
4. Boivin JC, Mairesse G. Recent material developments in fast oxide ion conductors. *Chem Mater* 1998;**10**:2870–88.
5. Jurado JR, Moure C, Duran P, Valverde N. Preparation and electrical properties of oxygen ion conductors in the Bi_2O_3–Y_2O_3 (Er_2O_3) systems. *Solid State Ionics* 1988;**518**:28–30.
6. Fung KZ, Baek HD, Virkar AV. Thermodynamic and kinetic considerations for Bi_2O_3-based electrolytes. *Solid State Ionics* 1992;**52**:199–211.
7. Wachsman ED, Ball GR, Jiang N, Stevenson D. A structural and defect studies in solid oxide electrolyte. *Solid State Ionics* 1992;**52**: 213–8.
8. Chiang Y, Birnie DP, Kingery WD. *Physical ceramics: principles for ceramic science and engineering*. New Jersey: John Wiley & Sons, Inc.; 1997.
9. Esaka T, Mangahara T, Iwahara H. Oxide ion conductivity in the sintered oxides of the system Bi_2O_3–MO_2 (M=Ti, Sn, Zr Te). *Solid State Ionics* 1989;**36**:129–32.
10. Hoflund GB. Characterization study of oxidized polycrystalline tin oxide surfaces before and after reduction in H_2. *Chem Mater* 1994;**6**: 562–8.
11. Kargin YF, Nelyapina NI, Skorikov VM. System Bi_2O_3–SnO_2. *Physicochem Stud Equilib Solut* 1986:81–3.
12. Galakhov FY. *Phase diagrams of refractory oxide systems: a handbook*. Leningrad: Nauka; 1986. pp. 298–299.
13. Asryan NA, Koltsova TN, Alikhanyan AS, Nipan GD. Thermodynamics and phase diagram of the Bi_2O_3–SnO_2 system. *J Inorg Mater* 2002;**38**(11):1141–7.
14. Levin EM, Robbins R, McMurdie HF. Phase diagrams for ceramics. *Columbus: Am Ceram Soc* 1964:125–9.
15. Rao CNR, Subba Rao GV, Ramdas S. Phase transformations and electrical properties of bismuth sesquioxide. *J Phys Chem* 1969;**73**: 672–5.
16. Harwig HA, Gerards AG. The polymorphism of bismuth sesquioxide. *Thermochimica Acta* 1979;**28**:121–31.
17. Weng CH, Wei WCJ. Synthesis and properties of homogeneous Nb-doped bismuth oxide. *J Am Ceram Soc* 2010;**93**(10):3124–9.
18. Montgomery DC, Runger GC, Hubele NF. *Engineering statistics*. New Jersey: John Wiley & Sons, Inc.; 2007. pp. 137–215.
19. Jones RH, Knight KS. The Structure of γ-$Bi_2Sn_2O_7$ at 725 °C by high-resolution neutron diffraction: implications for bismuth(III)-containing pyrochlores. *J Chem Soc Dalton Trans* 1997;**15**:2551–5.